Simulation of Detachment of Specifically Bound Particles from Surfaces by Shear Flow

Suzanne C. Kuo,* Daniel A. Hammer,# and Douglas A. Lauffenburger*
*Department of Chemical Engineering, University of Illinois at Urbana-Champaign, Urbana, Illinois 61801, and #School of Chemical Engineering, Cornell University, Ithaca, New York 14853 USA

ABSTRACT The receptor-mediated adhesion of cells to ligand-coated surfaces is important in many physiological and biotechnological processes. Previously, we measured the detachment of antibody-coated spheres from counter-antibody- and protein A-coated substrates using a radial-flow detachment assay and were able to relate mechanical adhesion strength to chemical binding affinity (Kuo and Lauffenburger, *Biophys. J. 65*:2191–2200 (1993)). In this paper, we use "adhesive dynamics" to simulate the detachment of antibody-coated hard spheres from a ligand-coated substrate. We modeled the antibody-ligand (either counter-antibody or protein A) bonds as adhesive springs. In the simulation as in the experiments, beads attach to the substrate under static conditions. Flow is then initiated, and detachment is measured by the significant displacement of previously bound particles. The model can simulate the effects of many parameters on cell detachment, including hydrodynamic stresses, receptor number, ligand density, reaction rates between receptor and ligand, and stiffness and reactive compliance of the adhesive springs. The simulations are compared with experimental detachment data, thus relating measured bead adhesion strength to molecular properties of the adhesion molecules. The simulations accurately recreated the logarithmic dependence of adhesion strength on affinity of receptor-ligand recognition, which was seen in experiments and predicted by analytic theory. In addition, we find the value of the reactive compliance, the parameter which relates the strain of a bond to its rate of breakage, that gives the best match between theory and experiment to be 0.01. Finally, we analyzed the effect of varying either the forward or reverse rate constants as different ways to achieve the same affinity, and showed that adhesion strength depends uniquely on the equilibrium affinity, not on the kinetics of binding. Given that attachment is independent of affinity, detachment and attachment are distinct adhesive phenomena.

NOMENCLATURE

f_b	force required to break bond
g	gravitational constant
h	height of cell above surface
k_b	Boltzmann's constant
k_f	forward reaction rate
k_f^o	intrinsic forward reaction rate
k_r	reverse reaction rate
k_r^o	intrinsic reverse reaction rate
l_b	extent of stretch
t	time
Δt	time interval
z	distance of the center of the sphere from the surface
A_c	contact area between model cell and surface
A_d	dimensionless adhesion number
A_{rec}	receptor tip area
A_{123}	Hamaker constant
B_i	bond number in contact region
C	receptor/ligand complex density
D_{rec}	diameter of receptor tip
F_{gr}	gravity force
F_t	total force to detach cell from surface
F_{vdw}	van der Waals force
H	scaled height, $(z - a)/a$
K_A	equilibrium association constant
K_D	equilibrium dissociation constant
K_D^{2D}	surface/surface equilibrium dissociation constant
K_D^{3D}	solution/surface equilibrium dissociation constant
L_o	initial ligand concentration
N_L	ligand density
N_R	receptor density
P_b	probability of binding
P_r	probability of breakage
Q	volumetric flow rate
R_c	receptor number in contact area
R_{ch}	cell radius
R_T	number of receptors
S_c	critical shear stress
S_{min}	minimum allowable height above surface
T	temperature
T_{crit}	critical tension
V_i	translational velocity
$\mathbf{x}_b$	time-varying vector for bond
$\mathbf{x}_m$	vector of Cartesian coordinates of receptor end on cell surface

Received for publication 12 March 1996 and in final form 19 March 1997.

Address reprint requests to Dr. Daniel A. Hammer, Department of Chemical Engineering, 392 Towne Building, 220 S. 33rd Street, University of Pennsylvania, Philadelphia, PA 19104. Tel.: (215) 573-6761; Fax: (215) 573-2093; E-mail: Hammer@seas.upenn.edu.

Dr. Kuo's present address is Systemix, 3155 Porter Drive, Palo Alto, CA 94304. E-mail: skuo@stem.com.

Dr. Lauffenburger's present address is Department of Chemical Engineering, Massachusetts Institute of Technology, 66-444, Cambridge, MA 02139. E-mail: lauffen@mit.edu.

0006-3495/97/07/517/15 $2.00

$\mathbf{x}_o$	vector of Cartesian coordinates of receptor end on ligand-coated surface
$\mathbf{C}$	torque vector
$\mathbf{F}$	force vector
$\mathbf{R}$	distance vector
$\mathbf{U}$	velocity vector
$[\mathbf{M}]$	mobility matrix, used in calculating velocities
$[\mathbf{Q}]$	addition of log of rotation matrices
$[\mathbf{R}]$	rotation matrix
$[\mathbf{T}]$	transformation matrix

Greek

ε	London retardation wavelength
ϕ	spherical coordinate of receptor
$\dot{\gamma}$	shear rate
$\dot{\gamma}_c$	critical shear rate
η	conversion factor for equilibrium dissociation constant
λ	equilibrium separation distance for spring
μ	viscosity
θ	spherical coordinate of receptor
ρ_c	cell density
ρ_m	medium density
σ	spring constant
σ_{ts}	transition state spring constant
τ_{mv10}	scaled time to move distance of 10 radii
Ω_i	angular velocity

INTRODUCTION

Receptor-mediated cell adhesion under conditions of fluid flow plays a crucial role in many physiological and biotechnological processes. For example, leukocyte and tumor cell homing to particular tissues is accomplished by specific receptor interactions with endothelial ligands (Springer, 1990). Cell affinity chromatography, in which cells bind specifically to ligand-coated supports, can be used for depletion of tumor cells from bone marrow for autologous transplantation, enrichment of stem cells from the bone marrow or peripheral blood for allogeneic transplantation or for gene therapy, and isolation of fetal cells from maternal blood for genetic diagnosis (Berenson et al., 1986; Sharma and Mahendroo, 1980).

A long-standing issue in cell adhesion is how receptor-mediated cell/cell or cell/substratum adhesion strength is related to receptor/ligand binding affinity. Previously we measured the detachment of antibody-coated spheres from counter-antibody- and protein A-coated substrates using a radial-flow detachment assay. The results related chemical binding affinity of antibody-protein A binding to mechanical adhesion strength (Kuo and Lauffenburger, 1993). The experimental results were analyzed in terms of an existing theoretical model for cell adhesion by Dembo et al. (1988). Combined with an expression for adhesion energy density by Evans (1985), this model successfully described the data, showing in particular that mechanical adhesion strength depends logarithmically on receptor-ligand affinity.

However, there are several unresolved questions regarding these experiments and the applicability of Dembo and co-workers' analytic theory that require further exploration. The analytic theory was derived for deformable membranes, yet the experiments were performed with hard particles, leading to questions of whether the two are directly comparable. Furthermore, the analytic theory suggests that kinetics, the rates of association and dissociation, play no role in the strength of adhesion. The experiments did not explicitly test the role of kinetics. However, the role of kinetics in detachment, if any, should be established. Finally, the theory of Dembo and co-workers suggests that mechanical properties of the adhesion molecules, such as their stiffness and reactive compliance, do not affect the strength of adhesion, but only the rate of detachment. The dependence of detachment strength on molecular mechanical properties was not tested in the experiments, but needs to be tested further. To address these issues, we use adhesive dynamics (Hammer and Apte, 1992). Adhesive dynamics is a computer simulation method that allows us to calculate how a particle coated with adhesion molecules will bind to a ligand-coated substrate under the action of an external force. Adhesive dynamics includes the effects of parameters such as receptor number, ligand density, rates of reaction between receptor and ligand, their affinity of interaction, colloidal interactions between the cell and the surface, magnitude of fluid flow, and the mechanical properties of the adhesive bonds on adhesion. In this case, we are interested in how these parameters affect the detachment of particles that are bound to surfaces at steady state, a mimic of the procedure used in the experiments. Adhesive dynamics simulations then permit determination of the appropriate parameter values to describe the results of detachment experiments (Kuo and Lauffenburger, 1993). The comparison between adhesion dynamics and experiment provides a further test of the adhesive dynamics method. Finally, parameters in the simulation can be altered to determine the sensitivity of detachment to these parameters for the design or better understanding of cell adhesion.

MODEL FORMULATION

Model geometry and receptor distribution

The model geometry is shown in Fig. 1. Hammer and Apte (1992) used a microvilli-covered hard sphere, where the microvilli are randomly distributed on the surface using a hard-disk overlap algorithm, and the Poisson distribution was used to place the receptors on the microvilli. In this work, the hard-disk overlap algorithm was used to place receptors directly on the hard sphere, without the microvilli extensions. This more closely resembles the IgG-coated polystyrene system used in the experimental work (Kuo and Lauffenburger, 1993). All receptors are sufficiently close to the substrate for binding to occur. The sphere has radius R_{ch},

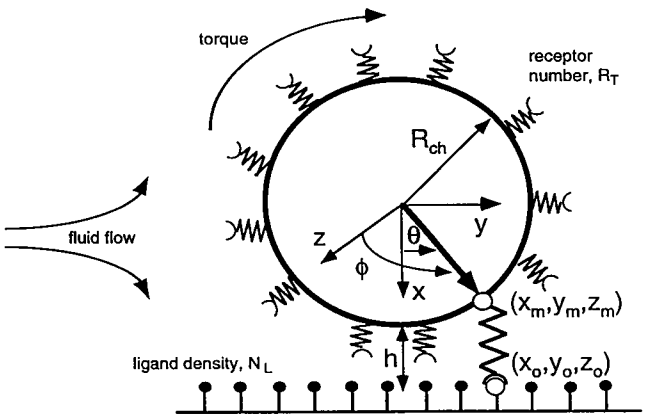

FIGURE 1 Model geometry and coordinate system. The cell is modeled as a hard sphere of radius R_{ch}, covered with R_T receptors. R_T receptors are randomly distributed over the cell surface, and the density of ligand on the substrate is assumed to be N_L. The positions of all receptors can be monitored with a Cartesian coordinate system, the origin of which is at the cell's center. The spherical coordinates are also used to identify receptor positions. The position of the end of each bond or tether is given by the vector (x_m, y_m, z_m). Similarly, the position of the bond on the substrate is given by (x_o, y_o, z_o). The distance h is a time-varying quantity, representing the separation distance between the sphere and the surface.

covered by R_T receptors. The receptor number in these simulations ranges from 5×10^4 to 3×10^5, and the receptors are randomly distributed on the surface. A ligand density of N_L molecules is assumed, and the density of these molecules is assumed to be in excess of the receptor density.

To characterize the system, two coordinate systems are used. A Cartesian system is centered on the cell. Each receptor, however, is given a unique position in spherical coordinates, determined by randomly placing the receptors on the cell surface. The translational and angular velocities are calculated in Cartesian coordinates. As the cell moves, the positions of the receptors relative to the surface change, requiring translations between Cartesian and spherical coordinates to provide the updated receptor positions. The ranges for the coordinates are $0 \leq \phi \leq \pi$ and $0 \leq \theta \leq 2\pi$. The receptors on the cell surface have coordinates in both coordinate systems.

The receptors are randomly distributed on the surface with the hard disk overlap algorithm (Appendix A). Unlike the receptors, the ligand on the planar surface is in excess and is uniformly reactive. Thus random distribution of ligand is not necessary for the simulation.

Spring model

The adhesion molecules are modeled as linear, Hookean springs with a spring constant σ. The force the bond exerts on the cell depends on the length of this "spring" or bond and on the spring constant. Therefore, the positions of the ends of the bond in Cartesian coordinates on both cell and ligand surfaces must be determined and tracked through time. These positions are stored as vectors, $\mathbf{x}_m = (x_m, y_m, z_m)$ and $\mathbf{x}_o = (x_o, y_o, z_o)$, where $\mathbf{x}_m$ is the position of the end of the tether attached to the cell and $\mathbf{x}_o$ is the position on the substrate. Because the sphere translates and rotates, the vectors $\mathbf{x}_m$ and $\mathbf{x}_o$ change with time. The bond can be described by a time-varying vector, $\mathbf{x}_b = \mathbf{x}_o - \mathbf{x}_m$.

Reaction kinetics and probabilities

Dembo et al. (1988) provide self-consistent kinetic rate expressions for a receptor/ligand bond modeled as a spring. The expressions relate the forward reaction rate k_f and the reverse reaction rate k_r to the vertical separation distance x_m between the receptor's position on the cell surface and the ligand-coated surface:

$$k_f = k_f^o \exp\left(-\frac{\sigma_{ts}(x_m - \lambda)^2}{2k_bT}\right) \quad (1)$$

$$k_r = k_r^o \exp\left(\frac{(\sigma - \sigma_{ts})(x_m - \lambda)^2}{2k_bT}\right) \quad (2)$$

where λ is the equilibrium separation distance for the spring, k_bT is the thermal energy (product of the Boltzmann constant and temperature), σ is the spring constant, and σ_{ts} is the transition state spring constant. The superscript ^{o} denotes rates of reactions that occur at the spring's equilibrium length. In Eq. 1, the forward reaction rate decreases as the distance deviates from equilibrium separation distances. The affinity k_f/k_r is given:

$$\frac{k_f}{k_r} = \frac{k_f^o}{k_r^o} \exp\left(-\frac{\sigma(x_m - \lambda)^2}{2k_bT}\right). \quad (3)$$

From these expressions, it is clear that the likelihood of a bond forming and remaining intact is reduced as the separation deviates from equilibrium. Hammer and Apte (1992) discuss the physical limitations of σ_{ts}, concluding that σ_{ts} will be finite and nonzero. In addition, the rate of bond breakage increases or decreases with extension, depending on the sign and magnitude of $(\sigma - \sigma_{ts})$. If the sign is positive, bond extension will lead to an accelerated rate of breakage ("slip bond"; Dembo et al., 1988). If the sign is negative, bond extension reduces the breakage and is called "catch bond." If the sign is zero, the bond is "ideal" and breaks at the same rate, regardless of extension. The magnitude of this difference and sign have a large effect on the adhesion of cells under conditions of fluid flow, as shown by Hammer and Apte (1992). To quantify this effect, we define a parameter called the reactive compliance, $F_\sigma = (\sigma - \sigma_{ts})/\sigma$, which is this difference scaled to the spring constant.

Given the expressions for the forward and reverse reaction rates (Eqs. 1 and 2), the probabilities for binding and breakage of an adhesive tether in a given simulation time step Δt can be calculated and sampled as described by Hammer and Apte (1992). The sampling is based on the probability of bond formation (breakage) P_b (P_r), which

depends on the reaction rate k_f (k_r) and time step Δt:

$$P_b = 1 - \exp(-k_f \Delta t) \quad (4)$$

$$P_r = 1 - \exp(-k_r \Delta t) \quad (5)$$

These probabilities are compared with a random number between 0 and 1 generated for each receptor (bond) to determine if the bond forms (breaks) during this time interval.

Force and torque calculations

The force a bond exerts on the cell is calculated from the length and orientation of the bond, using linear elasticity:

$$\mathbf{F}_b = \sigma(|\mathbf{x}_b| - \lambda)\mathbf{i}_b \quad (6)$$

The torque is then calculated from

$$\mathbf{C}_b = \mathbf{R}_b \times \mathbf{F}_b \quad (7)$$

where $\mathbf{R}_b$ is the vector from the bead center to the bond connection point. The net adhesive force and torque in each direction are calculated by summing these expressions over all bonds at every time point.

In addition to bond forces, the colloidal interactions between a sphere and a surface contribute to the total force. The contributions due to van der Waals, electrostatic, steric interactions, and gravitational body force are given in Appendix B.

The hydrodynamic shear forces and torques exerted by a passing fluid on an immobilized sphere in proximity to a plane wall were described by Goldman et al. (1967a,b).

Bond, colloidal, and shear forces are added to derive the vector of net forces acting on the bead:

$$\mathbf{F} = (F_x^b + F_x^c, F_y^b + F^s, F_z^b, C_x^b, C_y^b, C_z^b + C_z^s) \quad (8)$$

The superscripts b, c, and s indicate forces due to bonding, colloidal interactions, and shear, respectively.

Velocities

The net forces at each time step are then used to calculate the velocities of the sphere, using specific hydrodynamic functions that relate the applied forces and torques to the six components of translation and rotation (Brenner, 1961; Goldman et al., 1967a,b; Jeffrey, 1915). The vector of velocities is given by

$$\mathbf{U} = (V_x, V_y, V_z, \Omega_x, \Omega_y, \Omega_z) \quad (9)$$

The relationship between externally applied forces and torques and motions is written:

$$\mathbf{U} = [\mathbf{M}]\mathbf{F} \quad (10)$$

where [M] is the mobility matrix containing the hydrodynamic functions that depend on the separation distance between the cell and the surface, the cell radius R_{ch}, and the solution viscosity, μ. For motion of a sphere near a wall in viscous flow, this matrix is well characterized, as discussed in Hammer and Apte (1992).

Update of cell and receptor positions

When the bonds are initially formed, the position of the receptor ("bond end") on the substrate is directly below the receptor on the cell. Thus the x and y coordinates are identical. After the velocity is calculated for a given time step, the particle moves, and new positions (in both spherical and Cartesian coordinate systems) of the end points of each bond are updated for each time step. The Cartesian coordinates for the position of the receptors (x, y, z) are updated using the Cartesian translational velocities. The spherical coordinates of the receptors (θ, ϕ) are updated using the Cartesian angular velocities (Ω_i). The simulation is performed in the particle's reference frame, and thus, with each iteration, the position on the substrate changes according to the motion of the cell, creating an apparent convection of the substrate. The positions of the bond end on the substrate are updated using the translational velocities of the cell relative to the fixed surface. For these calculations, we developed a more accurate method for updating the positions of the receptor. Details of this method are found in Appendix C.

Dimensional analysis

Because the motion of the cells is driven by the external hydrodynamic flow, Hammer and Apte (1992) chose a time scale of $\dot{\gamma}^{-1}$, where $\dot{\gamma}$ is the shear rate. However, in the detachment experiments, there was no flow during attachment. Furthermore, during detachment, the shear rate varied for different locations in the flow chamber, so scaling with the shear rate is not practical. Thus time was scaled to the forward rate constant, multiplied by the ligand density.

Furthermore, scaling the forces to a shear rate, as was done in Hammer and Apte (1992), is not appropriate for these simulations. Therefore, forces are scaled to σR_{ch}, and torques are scaled to 4/3 σR_{ch}^2. Lengths are scaled to the radius of the sphere. The definitions and appropriate scales for the dimensionless groups are shown in Table 1. Estimates for values of the dimensional parameters are shown in Table 2, giving ranges suitable for leukocytes as well as for the latex bead system (Kuo and Lauffenburger, 1993). Leukocytes are a cell type that adheres to surfaces in the early events of the inflammatory response. The leukocyte ranges are presented in Table 2 for comparison with values measured or chosen for the spherical particles.

When the above dimensionless variables are used, the governing equations for the system can be rederived in dimensionless form for 1) kinetics of binding and breakage during a time step Δt, 2) dimensionless forces and torques due to the bonds, 3) dimensionless colloidal force, 4) dimensionless force and torque balances, and 5) translation of molecules. These balances are shown in Appendix D.

TABLE 1 Dimensionless parameters

Symbol	Definition	Scaling
τ	Scaled time	$\tau = tk_f^oN_L$
$\hat{x}_o$	Scaled Cartesion coordinate	$\hat{x}_i = \frac{x_i}{R_{ch}}, i = x, y, z$
δ_b	Scaled bond length	$\delta_b = \frac{\lambda}{R_{ch}}$
$\hat{h}$	Scaled bead height from surface	$\hat{h} = \frac{h}{R_{ch}}$
$\hat{V}_i$	Scaled translational velocity	$\hat{V}_i = \frac{V_i}{k_f^oN_LR_{ch}}$
$\hat{\Omega}_i$	Scaled angular velocity	$\hat{\Omega}_i = \frac{\Omega_i}{k_f^oN_L}$
α	Spring energy/fluid energy	$\alpha = \frac{\sigma}{6\pi\mu\dot{\gamma}R_{ch}}$
α'	Spring energy/fluid flow energy	$\alpha' = \frac{\sigma}{6\pi\mu k_f^oN_LR_{ch}}$
ν	Spring energy/thermal energy	$\nu = \frac{\sigma R_{ch}^2}{2k_bT}$
ν_{ts}	Transition state spring energy/thermal energy	$\nu_{ts} = \frac{\sigma_{ts}R_{ch}^2}{2k_bT}$
χ	Scaled forward reaction rate	$\chi = \frac{k_f}{k_f^o}$
χ_o	Intrinsic forward reaction rate/fluid flow rate	$\chi_o = \frac{\alpha}{\alpha'} = \frac{k_f^oN_L}{\dot{\gamma}}$
β	Scaled reverse reaction rate	$\beta = \frac{k_r}{k_f^oN_L}$
β_o	Scaled intrinsic reverse reaction rate	$\beta_o = \frac{k_r^o}{k_f^oN_L}$
F_σ	Reactive compliance	$F_\sigma = \frac{\sigma - \sigma_{ts}}{\sigma}$

Time interval

The choice of the time step for the attachment and the detachment phases is critical. If the time step was too large, multiple binding or breakage events could happen in one time interval, leading to unrealistic events, such as cycling of bond number or sudden breakage of all of the bonds. Smaller time steps were chosen to avoid these instabilities. However, small time steps lead to longer computer run time for the simulation. Depending on the forward rate constant, optimal time steps $\Delta\tau$ on the order of 10^{-6} were used for most of the simulations.

Attachment model verification

A series of attachment simulations were run initially to compare results with those of Hammer and Apte (1992). The translational velocities (V_i) and angular velocities (Ω_i) can be calculated as a function of dimensionless time, τ. These initial simulations showed that N_b, the number of bonds, and V_y, the velocity of the sphere in the direction of flow, are inversely related as expected. Maxima in N_b yield minima in V_y, and vice versa. These results are consistent with the results given by Hammer and Apte (1992), verifying the accuracy of the attachment code.

SIMULATION PROCEDURE

All computer programming and simulations were run on a Silicon Graphics IRIS Indigo workstation and an Iris Crimson server. The program was written and compiled in FORTRAN 77 and is available by request. Random numbers and seeds were generated with a portable random number generator provided in *Numerical Recipes* (Press et al., 1989). This random number generator has an infinite period in which different seeds (negative numbers) will generate different sequences. The function returns a uniform deviate between 0.0 and 1.0. In addition, the Graphics Library (GL) on the Indigo workstation was used to display the sphere and bond formation/breakage during the simulation; the Graphics Library provides subroutines for 2-D and 3-D color graphics and animation. The facilities at the Beckman Institute Visualization Laboratory (Urbana, IL) and at Silicon Graphics (Mountain View, CA) were used to videotape segments and store images from these animation sequences.

Attachment

To simulate the attachment step in the radial-flow detachment assay (RFDA) experiments, in which the beads were allowed to settle to the surface by gravity and no fluid flow was applied, zero shear rate was applied to the bead in the simulation. The attachment simulation was allowed to run until equilibrium was reached, or when the number of bonds did not change with time. Equilibrium attachment was reached within $\tau = 200$, equivalent to 6 ms for the cases in which $k_f^o = 5 \times 10^{-9}$ cm^2/s. At the end of the attachment simulation, the total number of bonds as well as the ϕ and θ positions of the bonds, the bead height above the surface, and the calculated bond forces and torques were stored in arrays for use as the initial conditions for the detachment phase of the simulation.

Detachment

Given the initial conditions for detachment as provided by the final conditions of the equilibrium attachment simulation, a shear rate was applied to the adhered bead, and time evolution of all extrinsic variables was monitored. The angular and translational velocities of the sphere were calculated from the forces and torques. If the fluid force was large enough, bonds were broken and the sphere traveled across the surface. The dimensionless distance that the bead traveled across the substrate was calculated from the translational velocity. Because small movements of the sphere on the order of the sphere radius or less are not necessarily indicative of attachment, we established a more realistic

Table 2 Estimates for dimensional parameters

Symbol	Definition	Value range	Simulation value	References
R_{ch}	Cell radius	2.5–50 μm	5 μm	Lawrence and Springer, 1991
A_{rec}	Area of receptor		10^{-13} cm^2	Cozens-Roberts, 1990
R_T	Number of receptors	10^4–10^7	5×10^4–3×10^5	Lawrence and Springer, 1991; Kuo and Luaffenburger, 1993
N_L	Ligand density	10^9–10^{13} #/cm^2	3.5×10^{12} #/cm^2	Lawrence and Springer, 1991; Kuo and Luaffenburger, 1993
λ	Equilibrium bond length	5–50 nm	25 nm	Springer, 1990
h_{init}	Initial height		2.6×10^{-6} cm	from antibody dimensions (Cozens-Roberts, 1990)
K	Affinity	10^7–10^{-3} cm^2	10^9–10^{13} cm^2	Bell, 1981; Lawrence and Springer, 1991
k_f^o	Forward reaction rate	10^{12}–10^{-7} cm^2/s	10^{-12}–10^{-8} cm^2/s	Hammer and Lauffenburger, 1987; Lawrence and Springer, 1991
k_r^o	Reverse reaction time		5×10^{-3} s^{-1}	Kuo and Luaffenburger, 1993
μ	Viscosity	0.01 g/cm-s	0.01 g/cm-s	Lawrence and Springer, 1991
$\dot{\gamma}$	Shear rate	50–400 s^{-1}	50–10,000 s^{-1}	Lawrence and Springer, 1991; Kuo and Luaffenburger, 1993
ρ_c	Cell density	1 g/cm^3	1 g/cm^3	Bongrand and Bell, 1984
ρ_m	Medium density	1.05–1.10 g/cm^3	1.05 g/cm^3	Bongrand and Bell, 1984
T	Temperature	277–310 K	298 K	
σ	Spring constant	0.5–5 dyne/cm	1–2 dyne/cm	Dembo *et al.*, 1988; Evans *et al.*, 1991
σ_{ts}	Transition state spring constant	−5–5 dyne/cm	0–2 dyne/cm	Dembo *et al.*, 1988
S_{min}	Minimum height above surface		200 Å	Cozens-Roberts, 1990

criterion for detachment. If the sphere traveled 10 radii, we assumed that it detached. A series of different shear rates was applied to an adherent sphere. For each shear rate, the dimensionless time for detachment, τ_{mv10}, was calculated, starting at the highest shear rate (~10,000 s^{-1}) for which the time for detachment would be the shortest. A plot of time taken to travel the 10 radii versus shear rate was generated. We found this relationship could be well fit with an equation of hyperbolic form:

$$(\dot{\gamma} - \dot{\gamma}_c)\tau_{mv10} = A \tag{11}$$

where $\dot{\gamma}_c$ is the asymptotic limit and A is a constant. This asymptote is the critical shear rate, $\dot{\gamma}_c$, at which it takes infinite time to detach the bead. This correlates with the critical shear rate measured in the RFDA experiments.

GENERAL RESULTS

Attachment

We simulated attachment of particles under zero fluid shear rate to obtain the initial conditions for detachment. Various receptor numbers were simulated, resulting in an increase in equilibrium bond number as receptor number increases. We found that $\tau = 200$ is a sufficient length of time to reach steady-state attachment. In general, roughly 0.2% of all the receptors are bound to ligand at steady state. This bond fraction is dependent on ligand density and the contact area. The diameter of the region over which receptors were bound was roughly 0.5 μm, which, given the bead radius of 5 μm, is 0.25% of the total sphere surface area. This suggests that all receptors in the contact area were bound, consistent with the excess ligand density assumption.

Detachment

After steady-state attachment had been attained, different shear rates were applied to the particles, and the times for detachment were measured. Fig. 2 shows a sample simulation in which a high shear rate is applied (at $\tau = 1000$, where $\tau = 0$ represents initial contact with the surface) and the number of bonds decreases dramatically. A plot of velocity corresponding to these conditions would show zero velocity until the time at which detachment shear was applied ($\tau = 1000$), where the velocity increases as bonds are broken.

As mentioned previously, a criterion based on the displacement of the particle was used to assess detachment. This is generally superior to a criterion based on binding, because singly bound particles could be motionless, or multiply bound particles could be in motion. So binding is not a unique determinant of detachment.

Fig. 3 shows the scaled distance traveled as a function of time, for increasing shear rates. In this example, shear rates greater than or equal to 100 s^{-1} displace the particle a distance of many radii. However, a shear rate of 50 s^{-1} does not cause significant, if any, translational displacement of the sphere. Therefore, the critical shear rate, the shear rate against which the sphere can resist translation, falls between 100 s^{-1} and 50 s^{-1}. To determine the critical shear rate accurately, the time (τ) required to move a certain distance was determined. A distance corresponding to significant

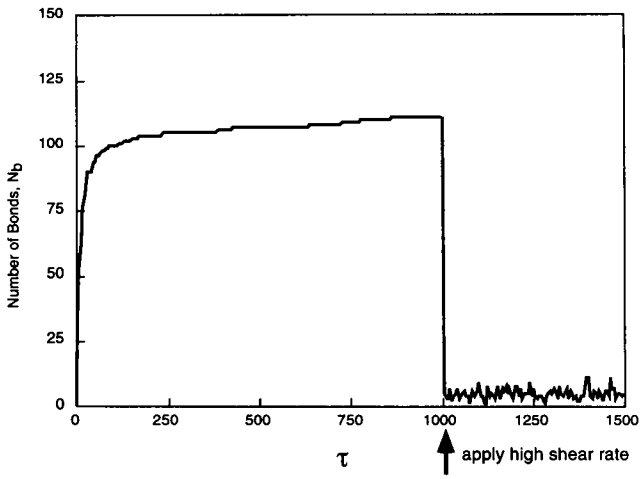

FIGURE 2 Equilibrium attachment followed by detachment with a high shear rate. The number of bonds formed increases with time until steady-state conditions are reached. Initially, zero shear flow is applied to represent adhesion without fluid flow. As the receptor number increases, the total number of bonds reaches equilibrium. Detachment flow is then applied ($\dot{\gamma} = 1 \times 10^4\ s^{-1}$) at $\tau = 1000$, and the number of bonds decreases. In this example, $k_f^o = 5 \times 10^{-9}$ cm^2/s, $k_r^o = 5 \times 10^{-3}\ s^{-1}$, and $F_\sigma = 0.01$.

displacement of the particle, 10 radii, was used. The times for displacement as a function of shear rate are well fit with the hyperbolic form given in Eq. 11, where $\dot{\gamma}_c$ is the asymptotic limit and A is a constant. This asymptote defines the critical shear rate, $\dot{\gamma}_c$.

Dependence on receptor number, R_T

Fig. 4 shows the results for detachment simulations (τ_{mv10} versus $\dot{\gamma}_c$) for four different receptor numbers ($5 \times 10^4 \leq R_T \leq 3 \times 10^5$). As R_T increases, the curve shifts to the right, indicating a higher critical shear rate. This is expected

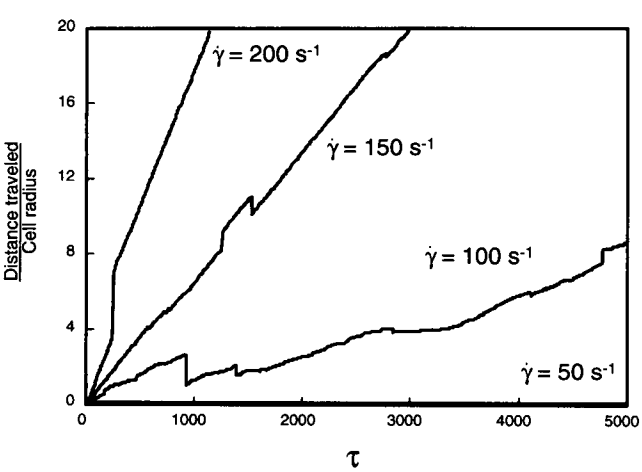

FIGURE 3 Scaled distance traveled by a sphere after varying detachment shear rates are applied. The distance traveled increases as the shear rate increases. Low shears, as shown in this example by $\dot{\gamma} = 50\ s^{-1}$, do not detach the sphere from the surface, and the distance traveled remains at zero.

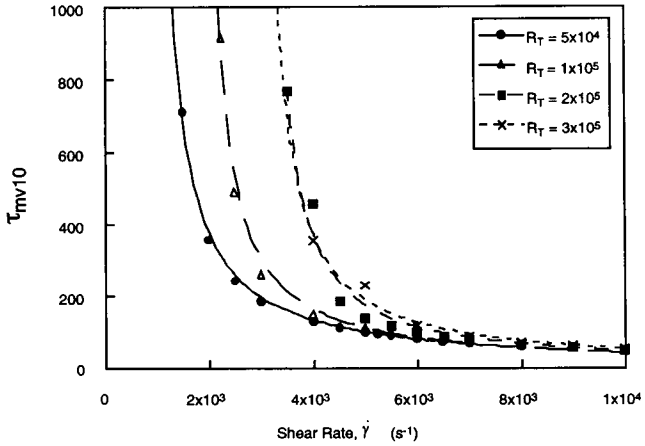

FIGURE 4 Time required for a sphere to travel a distance of 10 radii along the surface, for varying receptor number. Eq. 12 is fit to the data, where the asymptotic limit gives the critical shear rate. Increasing the receptor number increases the critical shear rate. In this example, $k_f^o = 5 \times 10^{-9}$ cm^2/s, $k_r^o = 5 \times 10^{-3}\ s^{-1}$, and $F_\sigma = 0.01$.

because particles with more receptors have more bonds in the contact region. Thus greater shear rates are required for detachment.

The critical shear rates, $\dot{\gamma}_c$, can be plotted as a function of receptor number. Fig. 5 shows the critical shear rate as a function of R_T for $F_\sigma = 0.01$. The critical shear rate increases with receptor number. At low receptor number, the critical shear rate is linear with the receptor number; at a higher receptor number, the critical shear rate reaches a saturable value. As we described (Kuo and Lauffenburger, 1993), the slope of the critical shear rate rate versus the receptor number curve at low receptor number gives the

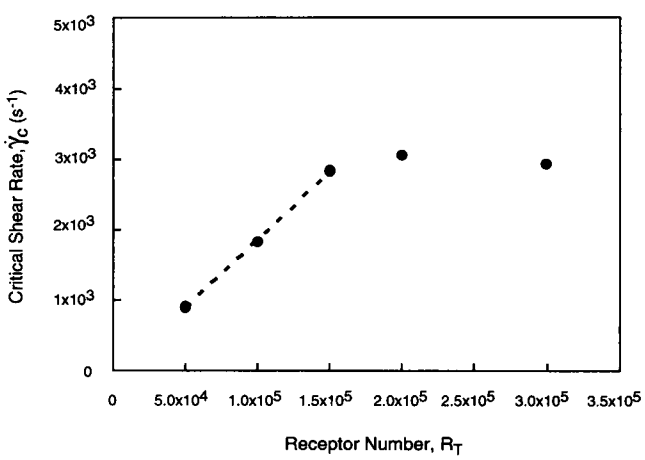

FIGURE 5 Determination of strength of binding per molecule. At low receptor number, the critical shear rate as a function of receptor can be fit by a straight line. The slope indicates the specific adhesion strength. The intercept (at low R_T) is a measure of the nonspecific adhesion. In this example, $k_f^o = 5 \times 10^{-9}$ cm^2/s, $k_r^o = 5 \times 10^{-3}\ s^{-1}$, $F_\sigma = 0.01$, and the slope equals 0.019. For the R_T values between 5×10^4 and 1.5×10^5, the linear fit is given by a correlation coefficient $R = 0.99$.

strength of adhesion molecules. Fig. 5 also shows the linear curve fit to the data in the linear regime.

These sample simulations illustrate the analysis method used for all simulations to determine the critical shear rate, $\dot{\gamma}_c$. As with the RFDA experiments, the critical shear rates are determined for several receptor numbers. The slope of critical shear rate versus receptor number is then determined for the particular values of k_f^o, k_r^o, K_D, and F_σ. To compare to critical shear stress reported in the RFDA experiments, we multiplied the critical shear rate by the solution viscosity.

Computer animation

The computer graphics and animation were used to observe the formation and breakage of bonds as well as the sphere's rotation and translation along the surface during detachment. In Fig. 6 we show several snapshots of the contact region between the bead and the substrate that provide insight into the mechanism of adhesion and detachment. Fig. 6 *A* shows the binding at $\tau = 200$ for an attached particle at steady state. At equilibrium, 191 bonds are formed. Fig. 6 *B* shows binding of the same particle after initiating a flow of $\dot{\gamma} = 10{,}000\ s^{-1}$. The radial line segment was normal to the substrate at steady state; its rotation off the normal illustrates a slight rotation of the sphere after the initiation of flow. The bond number has decreased to 141. Fig. 6 *C* shows the same particle at a later time. Now the particle is translating over the surface much more quickly, and the bond density has decreased to 38. Fig. 6 *D* illustrates a particle that was bound at steady state as in Fig. 6 *A*, but was exposed to a lower rate of shear of $300\ s^{-1}$, insufficient to dislodge the particle. Note that the level of binding actually increases to 297 after exposure to flow, because of the small rotation of the particle and the compression at the front edge of contact, which brings a greater fraction of the particle surface in contact with the substrate, leading to more binding.

SPECIFIC RESULTS

Dependence on the spring constant

The bonds are treated as adhesive springs; thus their stiffness is characterized by a spring constant σ. The spring constant can be varied while maintaining a constant reactive compliance F_σ, the fraction of the energy devoted to bond strain that is actually devoted to breaking the tethers. A value for F_σ of 0.01 is chosen while varying σ, allowing the

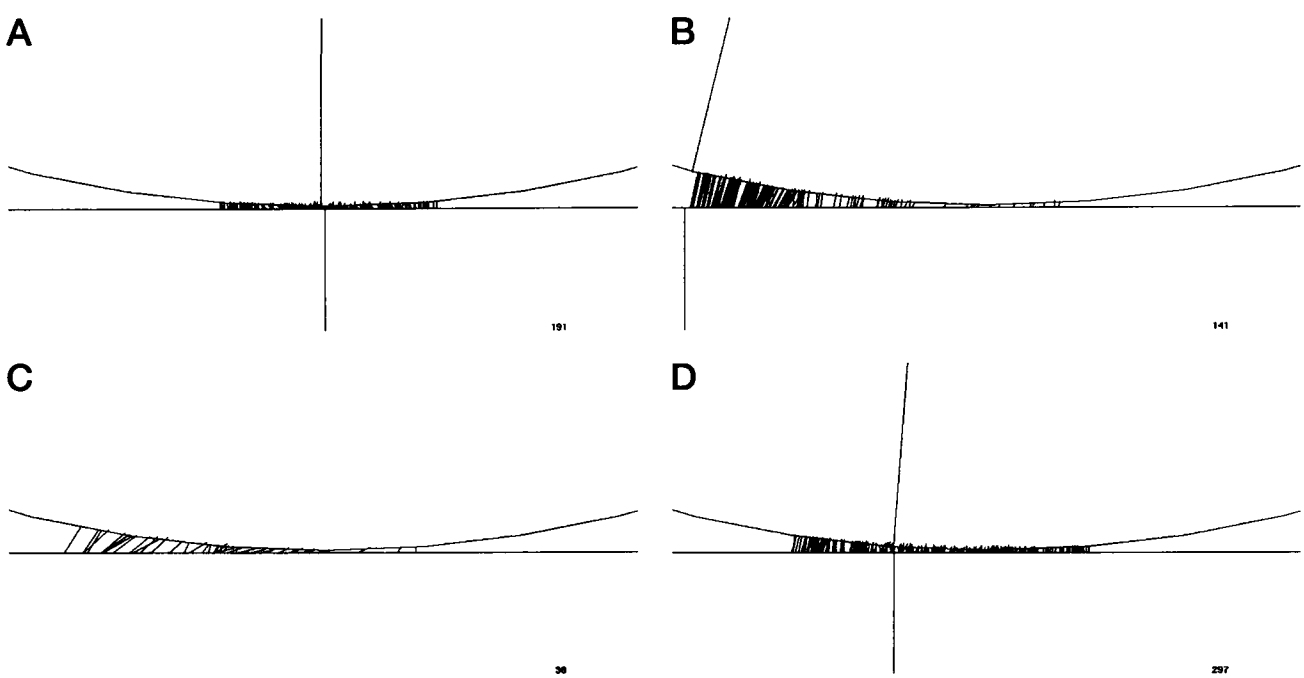

FIGURE 6 (*A*) Graphic representation of the contact zone for a particle attached at steady state. Bond formation has reached steady state by $\tau = 200$, and the bead is stably attached. This state is the initial condition for detachment. In this example, the bead has 10^5 receptors and 191 bonds have formed, as indicated by the number in the lower right corner. The parameters for this example are $k_f^o = 5 \times 10^{-9}\ cm^2/s$, $k_r^o = 5 \times 10^{-3}\ s^{-1}$, and $F_\sigma = 0.01$. (*B*) Graphic representation of bond formation in the contact zone immediately after application of flow. Detachment fluid flow ($\dot{\gamma} = 10^4\ s^{-1}$) has been applied to the adherent bead of *A*. Bonds in the rear of the sphere are extended as the sphere rolls forward along the substrate. The number of bonds at the time of the snapshot, detachment $\tau = 201$, is 141, as shown in the lower right corner. (*C*) Graphic representation of the contact zone well after flow has been applied: incipient detachment. Fluid flow ($\dot{\gamma} = 10^4\ s^{-1}$) has been applied to the adherent bead shown in *A*. A snapshot is taken at $\tau = 203$, a time later than shown in *B*. Fewer bonds (38) remain, and the sphere has rolled forward along the substrate. (*D*) Graphic representation of the contact zone after applying a low shear rate insufficient for detachment. A lower detachment fluid shear rate ($\dot{\gamma} = 300\ s^{-1}$) has been applied to the bead of *A*, which is bound at steady state. The fluid shear stress is insufficient to dislodge the particle from the surface. A snapshot is taken at $\tau = 222$, and fluid flow was applied at $\tau = 200$. Bonds are formed as the sphere rotates slightly forward to accommodate the external shear. At this time, 297 bonds have formed.

transition state spring constant σ_{ts} to vary appropriately. This isolates the effects of the spring constant on detachment. To demonstrate the effect of σ on detachment, we doubled σ to 2 dynes/cm. The critical shear rates are compared to the values obtained from simulations in which σ = 1 dyne/cm (Fig. 7). The critical shear rates in the linear regime are the same for σ = 1 dyne/cm and σ = 2 dynes/cm, and thus the slopes are identical. Therefore, the slope of the curve of critical shear rate versus receptor number at low receptor number is unaffected by spring stiffness. However, the saturation levels are different for the different values of the spring constant, with stiffer springs leading to lower values of the critical shear rate at high receptor number.

Dependence on reactive compliance

The reactive compliance, F_σ, further characterizes the bond micromechanics. This quantity is a fraction of the energy of bond strain that is actually devoted to breaking tethers. Hammer and Apte (1992) showed that decreases in F_σ lead to an increase in adhesiveness for cell attachment under flow conditions. It is desirable to study the effects of the reactive compliance on detachment. We illustrate the results for three different values of F_σ: 0.005, 0.01, and 0.02, where the spring constant σ was maintained at 1 dyne/cm and the transition state spring constant σ_{ts} varied from 0.995 to 0.98. We found that F_σ = 0.005 gives the highest critical shear rate. This agrees well with Hammer and Apte's (1992) results for attachment, in which greater adhesiveness corresponds to lower values of F_σ. Thus the detachment results illustrate that the reactive compliance is an important determinant of detachment.

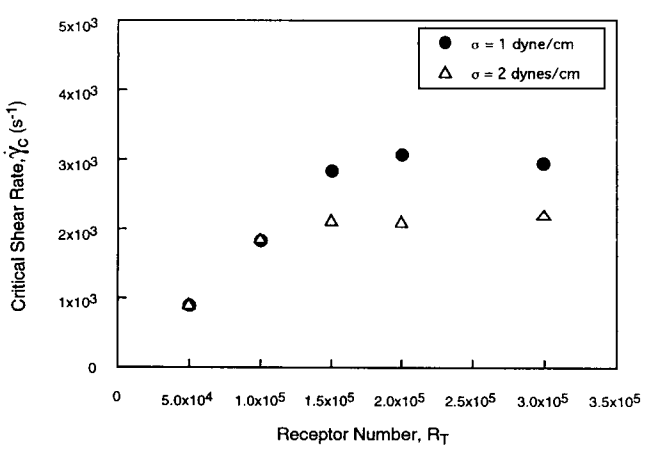

FIGURE 7 Critical shear versus receptor number for both σ = 1 and 2 dynes/cm and F_σ = 0.01. At low R_T, the critical shear as a function of R_T can be fit with a linear function to obtain the specific adhesion strength. The maximum critical shear at high receptor number depends on the spring constant. However, the specific adhesion strength does not differ for the different values of σ. In this example, $k_f^o = 5 \times 10^{-9}$ cm^2/s, $k_r^o = 5 \times 10^{-3}$ s^{-1}, and F_σ = 0.01.

We varied the receptor number and determined the critical shear rate for three different values of F_σ. The critical shear rates are plotted as a function of R_T for different F_σ. This is shown in Fig. 8. Again, the critical shear rate reaches a saturable value at high R_T ($R_T \geq 2 \times 10^5$). For F_σ = 0.005, a maximum critical shear rate appears to occur with R_T. Only data in the linear regime of the critical shear rate versus R_T plot are used to determine the molecular strength of adhesion. Just as Hammer and Apte (1992) concluded that the adhesiveness is greater for lower values of F_σ in attachment simulations, the lower values of F_σ correspond to higher specific adhesion strengths, as indicated by the greater slope of the critical shear rate versus R_T curve.

Dependence on equilibrium dissociation constant

Again, we examine detachment as a function of the equilibrium dissociation constant, the ratio of the rate constants. We varied the dissociation constant K_D in two ways: 1) by maintaining a constant forward reaction rate and varying the reverse rate, or 2) by maintaining a constant reverse reaction rate and varying the forward rate. We show how the slope of the critical shear rate versus receptor number depends on the equilibrium dissociation constants. The analytical result is also displayed as a point of reference, with parameters obtained from the curve fit of Dembo's model to the experimental data (Dembo et al., 1988).

Briefly, the experimental adhesion strength data (Kuo and Lauffenburger, 1993) can be analyzed in terms of a theoretical treatment previously offered by Dembo et al. (1988). The model is derived from a mechanical force balance on a peeling interface, allowing for stress distribution within the contact region, with the greatest stress acting on bonds at the perimeter of the region. The treatment specifies that the bond association and dissociation rate constants may be altered by input of energy, by a strain-

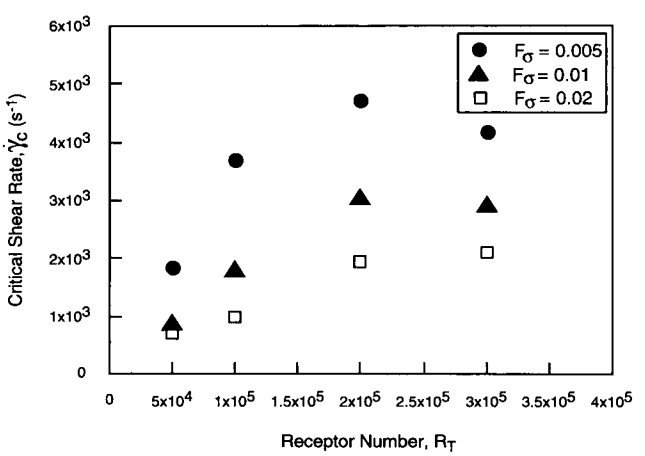

FIGURE 8 Critical shear versus receptor number for F_σ = 0.005, 0.01, and 0.02. An asymptotic value of critical shear is reached as the receptor number increases for each value of F_σ. The specific adhesion strength and the asymptotic value at high shear increase with decreasing F_σ. In this example, $k_f^o = 5 \times 10^{-9}$ cm^2/s, $k_r^o = 5 \times 10^{-3}$ s^{-1}, and σ = 1 dyne/cm.

dependent phenomenon. Dembo et al. define the critical tension T_{crit} as the value required to just begin peeling of a cell surface from the adhesion substratum. A mechanical force balance leads to an expression for T_{crit}:

$$T_{crit} = \frac{k_B \theta N_R \ln\{1 + (N_L/K_D)\}}{1 + \cos\alpha} \quad (12)$$

where k_B is Boltzmann's constant, θ is the absolute temperature, N_L is the substratum ligand density, α is the front angle between the membrane and the surface, and N_R is the cell receptor density. The surface energy for bonding between the membrane and the surface is equal to the numerator on the right-hand side of the equation and can be equated to an expression by Evans (1985) for the adhesion density, giving

$$\frac{F_t}{R_c} = \frac{2k_B\theta}{l_b} \ln\left\{1 + \frac{N_L}{K_D}\right\} \quad (13)$$

where l_b is the extent of stretch required to reach the peak force, F_t is the total force needed to detach a bead/cell from the surface, and R_c is the receptor number in the contact region. Details can be found in Kuo and Lauffenburger (1993). The main result is that the analytical model and the experimental data show that adhesion strength is proportional to the logarithm of the bond affinity.

Dependence on reverse rate constant

The forward rate constant was held constant ($k_f^o = 5 \times 10^{-9}$ cm^2/s) while the reverse rate constant was varied ($k_r^o = 1 \times 10^{-3}$ to 5×10^{-1} s^{-1}) to observe the effects of the reverse rate on detachment. This variation of the reverse rate constant gave dissociation constants K_D ranging from 3×10^{-13} M to 1.5×10^{-10} M. We performed simulations in which k_r^o was reduced five-fold to 1×10^{-3} s^{-1}, while maintaining constant k_f^o. The saturation behavior was again observed in the shear rate versus receptor number for a range of F_σ values, so the linear curve fit was performed on the data at low R_T. When we examined the effects of the two different values of k_r^o (5×10^{-1} s^{-1} and 1×10^{-3} s^{-1}) on the critical shear rates, the lower reverse rate constant gave the larger slope. Because the reverse rate constant affects the dissociation constant, these results also indicate that the lower dissociation constant, or higher affinity, gives a larger slope.

Fig. 9 shows the slopes as determined from the plots of critical shear rate versus receptor number, for a range of K_D, obtained by varying either the reverse or forward rate constant. Shown in this figure are the results for the three different values of the reactive compliance, F_σ. The slope decreases with increasing $\ln(K_D)$. The curves representing the different F_σ are similar, with higher values of F_σ giving smaller slopes. Therefore, the critical shear rate is uniquely determined by K_D and does not depend on the apportioning of dissociation constant between on and off rates.

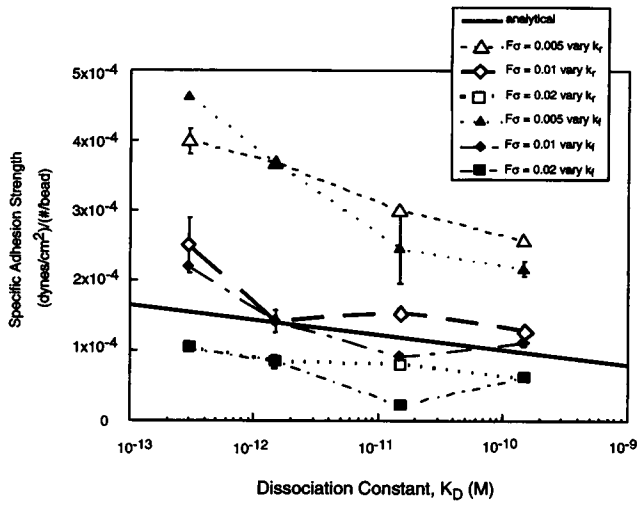

FIGURE 9 Effect of forward and reverse rate constants on specific adhesion strength. The specific adhesion strength for different F_σ are shown over a range of dissociation constants, obtained by 1) varying k_r^o while maintaining k_f^o at 5×10^{-9} cm^2/s and 2) varying k_f^o while maintaining k_r^o at 5×10^{-3} s^{-1}. The solid line represents the analytical expression given by Dembo and co-workers (1988), fit to experimental data.

Dependence on forward rate constant

A similar set of simulations was generated, maintaining the reverse rate constant ($k_r^o = 5 \times 10^{-3}$ s^{-1}) and varying the forward rate constant ($k_f^o = 2.5 \times 10^{-8}$ to 5×10^{-11} cm^2/s) to observe the effects on detachment. Fig. 9 shows the slopes as determined from the plots of critical shear rate versus receptor number. The forward rate constant was varied to obtain the different dissociation constants K_D, ranging from 3×10^{-13} to 1.5×10^{-10} M. Shown in this figure are the results for the three different values for F_σ. As before, the slope decreases with $\log(K_D^{-1})$. The curves representing the different F_σ are similar, with higher values of F_σ giving smaller slopes.

Heterogeneity

The effects of receptor position heterogeneity on the critical shear rate can be examined by using a different distribution of the receptors on the surface. For a series of 10 different seed values for distribution, only 0.4% variation in the critical shear rate was obtained. Thus performing the simulation for a single bead is an excellent approximation for a heterogeneous population of receptor-coated spheres.

Receptor number heterogeneity was also examined to observe the effects on the critical shear rate. When a coefficient of variation (CV) of 0.26 (Saterbak et al., 1993) was used for the receptor number, attachment and detachment were simulated for the receptor numbers, with one standard deviation greater or less than the mean. Simulations of detachment were performed for spheres with a mean receptor number of 10^5. Then the simulation was repeated for spheres with receptor numbers one standard deviation from

the mean. The CV in the critical shear rates for these simulations, as determined from the asymptote of the time (to move a distance of 10 radii) versus shear rate, ranged from 0.21 to 0.27, consistent with the receptor number deviation. This deviation, due to receptor number heterogeneity, was seen in all shear rate measurements. Because the simulation is rigorously dependent on the receptor number, it can be assumed that heterogeneity in R_T will affect the critical shear stress.

COMPARISON TO EXPERIMENT

Previous experimental data

Previously we have shown that the adhesion strength can be measured as a function of affinity of the receptor-ligand pair, using a radial-flow detachment assay (Kuo and Lauffenburger, 1993). We used latex polystyrene beads coated with biological molecules as a model for biological cells. The beads allowed easy and systematic manipulation of the type and number of proteins on the surface. Animal immunoglobulin G antibodies (IgG) were chosen for the receptor linked to the bead surface. Protein A (SpA), a cell wall constituent of *Staphylococcus aureus*, was chosen as the complementary ligand. Flow cytometric and radiolabel techniques were used to measure the equilibrium dissociation constant, K_D, between IgG and SpA. Most importantly, alteration of medium pH or use of different animal species as IgG sources permitted the variation of K_D over three orders of magnitude.

Adhesion strength was determined from measurement of the critical shear stress for detachment of beads from the coated glass substratum in the radial fluid flow chamber, following the method of Cozens-Roberts et al. (1990). Shear stress values were converted to total force by using an analysis of the translational force and rotational torque for a spherical particle near a surface (Hammer and Lauffenburger, 1987; Goldman et al., 1967a,b).

We found the adhesion strength per molecule (specific adhesion strength) to be proportional to the logarithm of the equilibrium dissociation constant, with a lower dissociation constant (greater bond affinity) corresponding to a higher slope (greater adhesion strength). These experimental results were examined in terms of a theoretical relation combining analyses by Dembo et al. (1988) and Evans (1985). This relation predicts a logarithmic dependence of adhesion strength on bond affinity. The experimental data were in accord with this prediction.

Simulation and experimental results

The dynamic cell detachment simulation model developed in this work can be used to describe the experimental RFDA data. We obtained the same general trends for critical shear rate as a function of receptor number as in the experiments. As the receptor number increases, critical shear rate increases to an asymptotic level, at which increases in receptor number no longer contribute to increases in the shear rate required for detachment. In addition, the simulations have shown that systems with lower K_D reach saturation at a lower receptor number. This trend was seen experimentally by Kuo and Lauffenburger (1993).

Fig. 10 shows the results for the simulations, along with both the analytical prediction from Dembo's model and the experimental RFDA data. Qualitatively, excellent agreement between the simulation results and the analytical expression was obtained from first fitting the experimental data with Dembo's model, then fitting Dembo's model with the simulations. The slope varies logarithmically with K_D in the experiments, the theory, and the simulations.

Fig. 10 illustrates that a bond reactive compliance of 0.01 is most consistent with the experimental data. As shown in Fig. 9, a reactive compliance larger than 0.01 would underestimate adhesion strength, whereas a reactive compliance smaller than 0.01 would overestimate. This result implies that only a small fraction (1%) of the total energy in bond strain is actually devoted to breakage of the tether, and the remainder is devoted to the extension of the molecule.

DISCUSSION

A simulation method has been presented for receptor-mediated attachment and detachment of a receptor-coated hard sphere to ligand-coated surfaces under viscous shear flow. We used the method to examine the effects of surface chemistry and bond micromechanics on cell detachment, examining a single model cell at a time. In the model, we vary parameters such as receptor densities, binding equilibrium and kinetic constants, bond response to strain, and fluid detachment force.

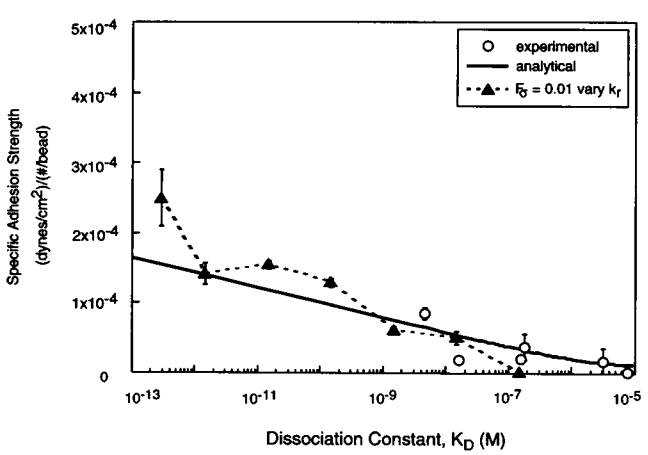

FIGURE 10 Comparison of simulation and experiment: specific adhesion strength as a function of K_D. The specific adhesion strength is calculated for different dissociation constants (▲) at $F_\sigma = 0.01$. These simulation results were obtained by varying the reverse rate constant while maintaining $k_f^o = 5 \times 10^{-9}$ cm²/s. ○, Experimental data for the SpA/IgG system. The solid line represents the analytical expression given by Dembo and co-workers (1988).

This method is an extension of Hammer and Apte's model for attachment of microvilli-coated hard spheres to surfaces under fluid flow. The objective of this calculation was to simulate the detachment of particles from surfaces. Fluid flow of varying shear stresses was applied to the system to detach the bead from the surface. Bond numbers, velocities, and forces were calculated and tracked through time. The critical shear rates were determined from measurements of the time taken to travel a distance of 10 bead radii, and a function was fit to the data to determine the asymptote. This limit gave the critical shear rate, or the shear rate at which infinite time is required for detachment. The slope of the critical shear rates versus receptor number is proportional to the specific adhesion strength, and the slopes for different sets of parameters can be compared.

The simulation results showed that the critical shear rate reaches a saturable level as receptor number increases (Figs. 5 and 8). This is in agreement with predictions of Hammer and Lauffenburger (1987) and with the experimental data of Kuo and Lauffenburger (1993). Increasing receptor number beyond that level is of no additional value for maintaining cell attachment under fluid flow. In addition, the simulations reproduced the observation that systems with high affinity binding molecules reached their plateau critical shear rates at lower receptor numbers than systems with lower affinity values. This is in agreement with experimental RFDA data, as observed with the SpA/IgG and avidin/biotin studies.

The model was used to examine the effects of micromechanics on detachment. The adjustable parameters were the spring constant and the reactive compliance. Variation in the spring constant by a factor of 2 did not produce different critical shear rates in the linear regime, and thus the slopes or specific adhesion strengths were identical (Fig. 7). However, increasing the spring stiffness did increase the asymptotic value of critical shear rate obtained at high receptor number. Thus, for these conditions, the spring stiffness alone does not influence the adhesion.

The simulations showed that an increase in the reactive compliance leads to a decrease in the critical shear rate and its slope as a function of receptor number (Fig. 8), or equivalently, to a decrease in the ability of the bead to remain adherent to the surface under flow. Because the reactive compliance is the fraction of the total spring energy devoted to the breakage of tethers under strain, it is expected that smaller reactive compliance leads to greater critical shear rates required for detachment. This behavior was observed in the simulation results. However, it will be important to experimentally determine the spring constant to be used in these simulations, currently a factor that can only be estimated. Until these parameters are experimentally measured, their effects can be simulated.

The model was used to examine the effects of the kinetic rate constants on detachment. A panel of simulations consisted of maintaining a constant forward reaction rate and varying the reverse rate to obtain a range of dissociation equilibrium constants. A second panel consisted of maintaining a constant reverse rate while varying the forward rate. For a given K_D value, the slopes of critical shear rate with receptor number were the same (within error), regardless of the set of kinetic parameters used (Fig. 9). This indicates that kinetics do not significantly affect detachment. Once adhered to the surface, the affinity controls the strength. This is different from what has been shown experimentally (Tempelman and Hammer, 1994) and theoretically (Hammer and Apte, 1992) for attachment under hydrodynamic flow; in this case, the kinetic forward rate dominates adhesion, and adhesion is independent of the affinity. These previous results and those of this paper suggest that attachment and detachment are distinct adhesive phenomena that are controlled by different features of adhesion molecules.

An additional result is the confirmation that adhesion strength depends on the logarithm of the dissociation constant, K_D. Previously we showed that our experimental results were well fit by a hybrid expression from theoretical work by Evans (1985) and Dembo et al. (1988), which predicted this logarithmic dependence. The simulations show the same functionality, and the dependence of adhesion strength on the dissociation constant seems to be consistent among theory, experiment, and simulation.

We were surprised by the value of the reactive compliance necessary to re-create the experimental data. To describe the experimental data, we found that F_σ must equal 0.01, a value larger than but close to that predicted by Hammer and Apte (1992) as being necessary for selectin bonds to permit neutrophil rolling. We must measure this parameter in many different systems of different functionality before reaching conclusions about its value. However, dissociation depends on the exponential of F_σ multiplied by the square of the strain on the molecules, so dissociation is a strong function of F_σ. Hence it may be that small changes in F_σ lead to large changes in dissociation and hence in receptor function.

In conclusion, we have developed a dynamic, probabilistic computer simulation for the detachment of antibody-coated hard spheres from a ligand-coated substrate. The antibody-ligand bonds were treated as adhesive springs. The distribution of receptors on the sphere and the forward and reverse reactions between receptor and ligand were simulated by using random number sampling of appropriate probability functions. The model simulated the effects of many parameters on cell detachment, including hydrodynamic stresses, receptor number, ligand density, reaction rates between receptor and ligand, and stiffness and reactive compliance of the adhesive springs. Adhesive dynamics may be easily modified to incorporate more realistic models for molecular rheology, once those models are elucidated. The simulations accurately represented the experimental data, re-creating the logarithmic relationship between adhesion strength and the dissociation constant of the adhesion molecules. In addition, the model predicted that a critical modulating parameter of detachment is the reactive compli-

ance, which relates the strain of a bond to its rate of breakage.

APPENDIX A: RECEPTOR DISTRIBUTION

The spherical coordinates (ϕ and θ) of the receptor being placed on the surface of a sphere are generated by random sampling, using

$$\phi = rdm\#_1 \cdot \pi$$
$$\theta = rdm\#_2 \cdot 2\pi \qquad \text{(A.1)}$$

where the random numbers are drawn from a uniform distribution from 0 to 1. Each receptor, the area of which is represented by a disk, is placed on the surface after comparing the new randomly generated ϕ and θ positions with all existing receptor locations. If overlap between the disk of the new receptor and any preexisting receptor exists, then the receptor is rejected. Otherwise, the receptor is accepted and the values are added to the position arrays of increasing θ, with R_T total numbers. A corresponding ϕ array is produced. This presorted θ array allows isolation of a local area of the cell surface and the receptors in it, with great saving of computer run time. Details of the implementation of the hard-disk overlap algorithm are given in Kuo (1994).

APPENDIX B: COLLOIDAL FORCES

The van der Waals force is an attractive charge interaction between polarizable molecules. The analysis of Dabros and van de Ven (1983) is followed for calculation of the van der Waals attraction force. For a colloidal particle near a surface under well-controlled hydrodynamic conditions, Dabros and van de Ven give the dispersion interaction force by an approximation (Suzuki et al., 1969):

$$F_{vdw} = -A_d \frac{\bar{\varepsilon}(\bar{\varepsilon} + 22.232H)}{H^2(\bar{\varepsilon} + 11.116H)^2} \qquad \text{(B.1)}$$

where A_d is the dimensionless adhesion number, defined as

$$A_d = \frac{A_{123}}{6k_bT} \qquad \text{(B.2)}$$

A_{123} is the Hamaker constant for interactions between media 1 and 2 in 3, a value estimated to be 2×10^{-20} J. This value was calculated on the basis of literature data on Hamaker constants of glass, water, and latex (Dabros and van de Ven, 1983). In Eq. B.1, $\bar{\varepsilon}$ is ε/R_{ch}, where ε is the London retardation wavelength. An estimate for $\bar{\varepsilon}$ is 0.4 (Dabros and van de Ven, 1983). Finally, in Eq. B.1, H is $(z - R_{ch})/R_{ch}$, where R_{ch} is the particle radius and z is the distance of the center of the sphere from the surface.

The gravitational body force is given by

$$F_{gr} = \frac{4}{3}\pi(\rho_c - \rho_m)R_{ch}^3 g \qquad \text{(B.3)}$$

where ρ_c is the cell density, ρ_m is the medium density, and g is the gravitational constant.

Two other major forces exist in biological systems at distances from 50 to 250 Å. The electrostatic force is usually a repulsive force, given that the surface charges are of the same sign. The steric stabilization force occurs because of the overlap of molecular chains (Bongrand and Bell, 1984) or, equivalently, two polymer coats. The water of hydration is pushed out and a repulsive force results as the water displays an osmotic tendency to return. The steric and electrostatic repulsive forces are modeled as a step function, which essentially prevents the bead from coming closer than a distance S_{min} to the surface, where S_{min} is the location of the step. This implies that the contribution to the total force from the steric and electrostatic forces is zero for bead/surface distances greater than S_{min} and infinity for distances less than S_{min}. The infinite repulsive force implies a minimum distance between the sphere and the surface. This limit for approach is included in the simulation to represent the steric and electrostatic forces.

APPENDIX C: TRANSFORMATIONS

Hammer and Apte model microvilli-coated spheres with 6000 receptors, and run times on the computer for a single attachment simulation take about 4 h. The simulations in this paper are for beads covered with 10^5 receptors. Therefore, extensive modification of the attachment algorithm was needed to reduce computer run time. The main element requiring large amounts of computer run time consisted of stepping through the entire receptor arrays for all calculations, including checking for bond formation and updating to the new positions. Rather than updating the position of each of the receptors, which becomes a very large task when the arrays are 10^5 long, orthogonal basis vectors are tracked with time. Rather than all receptors, only these three basis vectors and the origin are transformed with time as the cell rotates and translates. Orthogonality is maintained over the duration of the simulation. The downward-pointing vector is determined from the transformation matrix, and a "patch" around this vector, rather than the entire receptor array, is examined for bond formation. As a result, only the ϕ and θ values in this patch are transformed to the appropriate values, keeping the array in the original basis set and significantly reducing computer run time. Details of the matrix mathematics of the transformations follow.

Three unit basis vectors (or axes) are used to describe the sphere. In Cartesian coordinates, the initial basis set is chosen to be the identity matrix:

$$[\mathbf{I}] = \begin{bmatrix} 1 & 0 & 0 \\ 0 & 1 & 0 \\ 0 & 0 & 1 \end{bmatrix} \qquad \text{(C.1)}$$

The matrix [I] contains the unit axes that describe the sphere in its original basis set. As the sphere moves in time, these three vectors are transformed. So, letting [T] be the transform matrix, where

$$[\mathbf{I}][\mathbf{T}] = [\mathbf{T}] \qquad \text{(C.2)}$$

gives the result that [T] contains the axes in the new, transformed base.

To find the region or patch on the sphere surface near the ligand surface, the downward-pointing vector in the current time step is found. The current downward-pointing vector is defined simply to be the unit x vector:

$$\mathbf{x} = \begin{bmatrix} 1 \\ 0 \\ 0 \end{bmatrix} \qquad \text{(C.3)}$$

This same vector must be defined in the original basis set. An inverse transform is performed, using

$$\mathbf{x}_o = \mathbf{x}[\mathbf{T}]^{-1} \qquad \text{(C.4)}$$

where $\mathbf{x}_o$ is the same vector, but in the original basis set. Conveniently, because [T] is orthogonal, the inverse of the matrix is just the transpose, and thus $\mathbf{x}_o$ is simply the first column of [T]. This vector defines a range of θ and corresponding ϕ values in which attachment and detachment are analyzed. Because the θ values are stored in the array by increasing value, a "slice" of the sphere is analyzed for attachment and detachment. Thus only a fraction of the entire array is checked for binding, saving tremendous amounts of computer run time.

To determine the patch size, an angle ζ is calculated from the geometry of the sphere near the surface. The height of the sphere above the surface is crucial in determining this angle. The patch region is set to be the area of the sphere within twice the length of the receptor from the sphere. Beyond this height, it is assumed that bonds cannot form. Using an antibody (240 Å) as the receptor and a height restriction of twice this size, the angle ζ can be determined.

An interesting issue arises when determining the transformation matrix [T] with each time iteration. With each iteration, the sphere experiences torques, and thus rotations, around each of the three axes. These rotations cannot occur sequentially, because the order affects the final result. For example, rotating 90° around the x axis, followed by rotating 90° around the y axis, gives a different result for the transform than performing the opposite order, around the y axis and then x. In terms of matrix transformations,

$$[\mathbf{R}]_x[\mathbf{R}]_y \neq [\mathbf{R}]_y[\mathbf{R}]_x \tag{C.5}$$

Rotations are not commutative. It is necessary to determine the matrix [R], where [R] is the result of the three rotations occurring simultaneously. Then [R] can be used to calculate the new transform matrix by

$$[\mathbf{T}]_n = [\mathbf{T}]_{n-1}[\mathbf{R}] \tag{C.6}$$

A closed-form solution for the simultaneous, triple rotation does exist and can be derived from integrating equation 8.5.4 of Frazer et al. (1947). The result is an expression for [R], in terms of the angles of rotation:

$$[\mathbf{R}] = \exp[\mathbf{Q}] \tag{C.7}$$

The matrix [Q] is given by

$$[\mathbf{Q}] = \begin{bmatrix} 0 & \omega_z & -\omega_y \\ -\omega_z & 0 & \omega_x \\ \omega_y & -\omega_x & 0 \end{bmatrix} \tag{C.8}$$

where ω_x, ω_y, ω_z are the rotations around the x, y, and z axes, respectively. Using the properties of exponentiation of a matrix (Frazer et al., 1947), we can derive the closed-form solution for the rotations:

$$[\mathbf{R}] = \exp([\mathbf{Q}]) = [\mathbf{I}] + \frac{\sin k}{k}[\mathbf{Q}] + \frac{1-\cos k}{k^2}[\mathbf{Q}]^2 \tag{C.9}$$

where

$$k = \sqrt{\omega_x^2 + \omega_y^2 + \omega_z^2} \tag{C.10}$$

(D. Asimov, personal communication).

The reader may find it interesting to see how Eq. C.6 relates to the rotation around each axis. Separating [Q] into its components, we obtain

$$[\mathbf{Q}] = [\mathbf{Q}]_x + [\mathbf{Q}]_y + [\mathbf{Q}]_z \tag{C.11}$$

where

$$[\mathbf{Q}]_x = \begin{bmatrix} 0 & 0 & 0 \\ 0 & 0 & \omega_x \\ 0 & -\omega_x & 0 \end{bmatrix}, \quad [\mathbf{Q}]_y = \begin{bmatrix} 0 & 0 & -\omega_y \\ 0 & 0 & 0 \\ \omega_y & 0 & 0 \end{bmatrix},$$

$$[\mathbf{Q}]_z = \begin{bmatrix} 0 & \omega_z & 0 \\ -\omega_z & 0 & 0 \\ 0 & 0 & 0 \end{bmatrix} \tag{C.12}$$

Using only the x component in Eq. C.6,

$$[\mathbf{R}]_x = \exp[\mathbf{Q}]_x = \begin{bmatrix} 1 & 0 & 0 \\ 0 & \cos\omega_x & \sin\omega_x \\ 0 & -\sin\omega_x & \cos\omega_x \end{bmatrix} \tag{C.13}$$

we arrive at the well-known transformation matrix for rotation about the x axis. Similarly, the y and z components are the rotations about their respective axes. We noted earlier that the rotations are not commutative- and, therefore, cannot be multiplied in any order to obtain the same result. However, the composite rotation matrix [R] does, in fact, use only commutative operations over x, y, and z:

$$[\mathbf{R}] = \exp([\mathbf{Q}]_x + [\mathbf{Q}]_y + [\mathbf{Q}]_z) \tag{C.14}$$

In summary, the transform matrix [T] is calculated using [R] (Eq. C.9), and the inverse or transpose of [T] is taken. The first column of [T] gives $\mathbf{x}_o$, the downward-pointing vector in the original basis set. This vector defines a neighboring range of θ and corresponding ϕ values in which attachment and detachment are analyzed. Maintaining a sorted and segmented θ array reduces the number of calculations performed, because only a fraction of the receptors are examined for binding.

APPENDIX D: DIMENSIONLESS GOVERNING EQUATIONS

When the dimensionless variables given in Table 1 are used, the governing equations for the system become

1) kinetics of binding and breakage during a time step Δt:

$$\chi = \exp(-\hat{\nu}_{ts}(\hat{x}_m - \hat{\delta})^2)$$

$$\beta = \beta_o \exp((\hat{\nu} - \hat{\nu}_{ts})(\hat{x}_m - \hat{\delta})^2)$$

$$P_b = 1 - e^{-\chi\Delta\tau}$$

$$P_r = 1 - e^{-\beta\Delta\tau} \tag{D.1}$$

2) dimensionless forces and torques due to the bonds, where forces are scaled to σR_{ch} and torques to 4/3 σR_{ch}^2:

$$\hat{F}_i = (|\hat{\mathbf{B}}| - \delta)\left(\frac{\hat{i}_o - \hat{i}_m}{|\hat{\mathbf{B}}|}\right); \quad i = x, y, z \tag{D.2}$$

$$\hat{C}_x = \frac{4}{3}[-\hat{F}_z \sin\phi_m \sin\theta_m - \hat{F}_y \cos\phi_m]$$

$$\hat{C}_y = \frac{4}{3}[\hat{F}_x \cos\phi_m - \hat{F}_z \sin\phi_m \cos\theta_m] \tag{D.3}$$

$$\hat{C}_z = \frac{4}{3}[\hat{F}_y \sin\phi_m \cos\theta_m - \hat{F}_x \sin\phi_m \sin\theta_m]$$

$$|\hat{\mathbf{B}}| = \sqrt{(\hat{x}_o - \hat{x}_m)^2 + (\hat{y}_o - \hat{y}_m)^2 + (\hat{z}_o - \hat{z}_m)^2} \tag{D.4}$$

3) dimensionless colloidal force:

$$\hat{F} = \hat{F}_{vdw} + \hat{F}_g$$

$$= -\frac{A_{123}}{6R_{ch}^2\sigma}\left[\frac{\bar{\varepsilon}(\bar{\varepsilon} + 22.232H)}{H^2(\bar{\varepsilon} + 11.116H)^2}\right] + \frac{4}{3}\frac{\pi}{\sigma}(\rho_c - \rho_m)R_{ch}^2 g \tag{D.5}$$

4) dimensionless force and torque balances:

force in x:
$$F_7(\hat{h})\hat{V}_x = \sum_b \hat{F}_x + \hat{F}_x^c$$

force in y:
$$-F_3(\hat{h})\hat{V}_y + F_1(\hat{h})\hat{\Omega}_z - \frac{1}{\chi_o}F_5(\hat{h})(1 + \hat{h}) = \alpha'\sum_b \hat{F}_y$$

force in z:
$$F_3(\hat{h})\hat{V}_z + F_1(\hat{h})\hat{\Omega}_y = -\alpha'\sum_b \hat{F}_z$$

torque in x:
$$F_8(\hat{h})\hat{\Omega}_x = \sum_b \hat{C}_x \qquad \text{(D.6)}$$

torque in y:
$$-F_4(\hat{h})\hat{V}_z - F_2(\hat{h})\hat{\Omega}_y = \alpha' \sum_b \hat{C}_y$$

torque in z:
$$\frac{1}{\alpha'} F_4(\hat{h})\hat{V}_y - \frac{1}{\alpha'} F_2(\hat{h})\hat{\Omega}_z = \sum_b \hat{C}_z - \frac{1}{2\alpha} F_6(\hat{h})$$

In these expressions, summation is over the bonds, designated b. These balances are derived in Hammer and Apte (1992). $F_i(\hat{h})$ are hydrodynamic functions. F_1 through F_6 are given by Goldman, Cox, and Brenner (Goldman et al., 1967a,b). F_7 is given by Brenner (1961), and F_8 is given by Jeffrey (1915). These expressions are used to find [**M**], the mobility matrix, and **U**, the velocities, through Eq. 10.

5) translation of molecules:
$$\frac{di_o}{dt} = -V_i, \quad i = x, y, z \qquad \text{(D.7)}$$

and 6) rotation of molecules using the transformation matrices (Appendix C).

The author thanks Mark Peercy of Silicon Graphics for his assistance in producing the images and Michael Peercy for his contributions to refining the computer code. This work was partially supported by a grant from the National Center for Supercomputing Applications, University of Illinois at Urbana-Champaign. DAH acknowledges support for this work from NIH HL 18208.

REFERENCES

Bell, G. I. 1981. Estimate of the sticking probability for cells in uniform shear flow with adhesion caused by specific bonds. *Cell Biophys.* 3:289–304.

Berenson, R. J., W. I. Bensinger, and D. Kalamasz. 1986. Positive selection of viable cell populations using avidin-biotin immunoadsorption. *J. Immunol. Methods* 91:11–19.

Bongrand, P., and G. I. Bell. 1984. Cell–cell adhesion: parameters and possible mechanisms. *In* Cell Surface Dynamics: Concepts and Models. A. S. Perelson, C. DeLisi, and F. Wiegel, editors. Marcel Dekker, Inc., New York. 459–493.

Brenner, H. 1961. The slow viscous motion of a sphere through a fluid toward a plane surface. *Chem. Eng. Sci.* 16:242–251.

Cozens-Roberts, C., J. A. Quinn, and D. A. Lauffenburger. 1990. Receptor-mediated adhesion phenomena: model studies with the radial-flow detachment assay. *Biophys. J.* 58:107–125.

Dabros, T., and T. G. M. van de Ven. 1983. A direct method for studying particle deposition onto solid surfaces. *Colloid Polym. Sci.* 261: 694–707.

Dembo, M., D. C. Torney, K. Saxman, and D. Hammer. 1988. The reaction-limited kinetics of membrane-to-surface adhesion and detachment. *Proc. R. Soc. Lond.* B234:55–83.

Evans, E. 1985. Detailed mechanics of membrane-membrane adhesion and separation. I. Continuum of molecular cross-bridges. *Biophys. J.* 48: 175–183.

Evans, E., D. Berk, and A. Leung. 1991. Detachment of agglutinin-bonded red blood cells. I. Forces to rupture molecular-point attachments. *Biophys. J.* 59:838–848.

Frazer, R. A., W. J. Duncan, A. R. Collar. 1947. Elementary Matrices and Some Applications to Dynamics and Differential Equations. Cambridge University Press, Cambridge.

Goldman, A. J., R. G. Cox, and H. Brenner. 1967a. Slow viscous motion of a sphere parallel to a plane wall. I. Motion through a quiescent fluid. *Chem. Eng. Sci.* 22:637–652.

Goldman, A. J., R. G. Cox, and H. Brenner. 1967b. Slow viscous motion of a sphere parallel to a plane wall. II. Couette flow. *Chem. Eng. Sci.* 22:653–660.

Hammer, D. A., and S. A. Apte. 1992. Simulation of cell rolling and adhesion on surfaces in shear flow: general results and analysis of selectin-mediated neutrophil adhesion. *Biophys. J.* 63:35–57.

Hammer, D. A., and D. A. Lauffenburger. 1987. A dynamical model for receptor-mediated cell adhesion to surfaces. *Biophys. J.* 52:475–487.

Jeffrey, G. B. 1915. On the steady rotation of a solid of revolution in a viscous fluid. *Proc. Lond. Math. Soc.* 14:327–338.

Kuo, S. C. 1994. Experimental and computational studies of receptor-mediated cell detachment in shear flow. Ph.D. thesis. University of Illinois at Urbana-Champaign, Urbana, IL.

Kuo, S. C., and D. A. Lauffenburger. 1993. Relationship between receptor/ligand binding affinity and adhesion strength. *Biophys. J.* 65:2191–2200.

Lawrence, M. B., and T. A. Springer. 1991. Leukocytes roll on a selectin at physiologic flow rates: distinction from and prerequisite for adhesion through integrins. *Cell.* 65:859–873.

Press, W. H., B. P. Flannery, S. A. Teukolsky, and W. T. Vetterling. 1989. Numerical Recipes: The Art of Scientific Computing (FORTRAN Version). Cambridge University Press, Cambridge.

Saterbak, A., S. C. Kuo, and D. A. Lauffenburger. 1993. Heterogeneity and probabilistic binding contributions to receptor-mediated cell detachment kinetics. *Biophys. J.* 65:243–252.

Sharma, S. K., and P. P. Mahendroo. 1980. Affinity chromatography of cells and cell membranes. *J. Chromatogr.* 184:471–499.

Springer, T. A. 1990. Adhesion receptors in the immune system. *Nature.* 346:425–434.

Suzuki, A., N. F. H. Ho, and W. I. Higuchi. 1969. Predictions of the particle size distribution changes in emulsions and suspensions by digital computation. *J. Colloid Interface Sci.* 29:552–564.

Tempelman, L. A., and D. A. Hammer. 1994. Receptor-mediated binding of IgE-sensitized rat basophilic leukemia cells to antigen-coated substrates under hydrodynamic flow. *Biophys. J.* 66:1231–1243.